Fuel 344 (2023) 128088

Contents lists available at ScienceDirect

Fuel

journal homepage: www.elsevier.com/locate/fuel

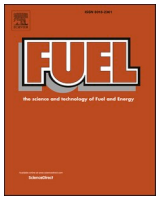

Full Length Article

Removal and mechanism analysis of NO_x emissions in carbon-free ammonia combustion systems with a secondary fuel injection

Tao Cai [a], Dan Zhao [a,*], Lin Ji [b], Avinash Kumar Agarwal [c]

[a] Department of Mechanical Engineering, College of Engineering, University of Canterbury, Private Bag 4800, Christchurch 8041, New Zealand
[b] Department of Chemistry, Capital Normal University, Beijing 100048, China
[c] Engine Research Laboratory, Department of Mechanical Engineering, Indian Institute of Technology Kanpur, Kanpur 208016, India

ARTICLE INFO

Keywords:
Ammonia combustion
NO_x emission mitigation
Secondary fuel injection
Kinetic effect

ABSTRACT

Ammonia, as a carbon-free renewable fuel of emerging interest, has the potential to substitute conventional fossil fuels. However, one challenge in utilizing such fuel is the risk of high NO_x (nitrogen oxide) emissions. This work clarifies how a secondary fuel injection strategy affects pollutant formation and pinpoints the underlying suppression mechanism. For this, a three-dimensional computational model involving a detailed ammonia/oxygen kinetic mechanism is established and validated with experimental data from the literature. Effects of the primary fuel flow rate, secondary fuel injection ratio $\Re$, and the dimensionless axial location of the secondary fuel injection ℓ on the emission behavior are evaluated in detail. Introducing such a strategy leads to an approximately 28% NO (nitric oxide) emissions reduction, mainly due to the chemical effect of NO reacting with NH_2 from NH_3 decomposition downstream of the secondary injection region. Increasing $\Re$ is associated with a lower NO emission but a higher NH_3 that is negligible or notable. Furthermore, varying ℓ is found to result in a slight change in the NO emission, whereas it greatly affects the NH_3 consumption. This work confirms the viability of applying a secondary fuel injection strategy to mitigate NO_x emissions without a negligible NH_3 penalty.

1. Introduction

Power generation and propulsion combustion devices operating with fossil fuels have been playing a vital role in daily human life but have also sparked serious challenges such as climate change and the energy crisis [1–3]. In a response to these issues, various sectors such as the energy and environment sectors have taken some effective actions and conducted proper cooperation [4,5]. Utilizing ammonia as an alternative renewable and carbon-free fuel offers a potential pathway toward reducing the carbon footprint of applications [6–8]. The following factors are responsible for a growing interest in using ammonia as fuel. Ammonia is a zero-carbon fuel that contains a large amount of hydrogen; it is, therefore, capable of replacing conventional fossil fuels. Additionally, such fuel is much more adaptive to the existing infrastructure, leading to the ease of transportation and storage.

Another merit of using such fuel is that ammonia can be readily produced with easy access using the well-established Haber-Bosch technology [9]. Meanwhile, the concept of producing green ammonia with renewable energy sources such as wind and solar power has recently been explored and is currently being evaluated [10–12]. Nonetheless, because of the low laminar burning velocity, burning ammonia directly is sluggish [13–15]. As a result, undesired flame dynamics such as pulsating flames and thermoacoustic instability could occur easily [16,17]. The high NO_x emissions from ammonia-fueled combustion are a limitation, primarily due to nitrogen atoms present in the fuel.

There have been extensive and concerted experimental and numerical efforts to circumvent these technical challenges to enable these combustion systems to run on ammonia. Approaches to enhance the flame speed are well established and documented, such as dual-fuel combustion and oxygen-enriched combustion [18–22]. Regarding the control technique of NO_x emissions, several comprehensive studies were focused on the application of selective catalytic reduction (SCR) and selective non-catalytic reduction (SNCR) [23–25]. These two techniques have frequently been applied in conventional power plants and internal combustion engines as an after-treatment technology to reduce NO_x emissions. They have proven extremely effective over a range of operating conditions.

Besides traditional ways to remove NO_x formation, several effective and feasible strategies can achieve this goal, specifically in the context of

* Corresponding author.
E-mail address: dan.zhao@canterbury.ac.nz (D. Zhao).

https://doi.org/10.1016/j.fuel.2023.128088
Received 23 January 2023; Received in revised form 20 February 2023; Accepted 5 March 2023
Available online 12 March 2023

ammonia-fueled combustion. The first one is based on the concept of varying thermodynamic properties [26,27]. Rich combustion is one of the most effective ways to minimize NO_x emissions due to the lack of O and OH radicals [28,29]. Still, it could be associated with leakage of NH_3, leading to low combustion efficiency. Thus, in ammonia-fueled combustion systems, slightly rich combustion is desirable. The heat losses from combustor outer walls are also shown to play a role in the NO formation [30]. Another method of potentially suppressing NO formation in ammonia-fueled systems involves elevating the initial pressure [31,32]. Furthermore, plasma-assisted combustion has been demonstrated as an effective technique to control NO_x emissions in addition to ignition and combustion improvements [33]. This was experimentally confirmed in the work of Choe et al. [34], who pointed out that the emission reduction effectiveness was dependent on the discharge power and voltage.

Co-firing combustion can function effectively as another potential way of suppressing NO_x emissions by properly alternating the mixture composition [35–40]. Zhang et al. [35] experimentally and numerically evaluated the NO_x performance in lean ammonia-doped hydrogen/air flames. The NO_x emissions were shown to increase first and then decrease by increasing the hydrogen volume fraction in the mixture. Ramos et al. [36] presented an experimental and kinetic analysis of NO_x emissions in ammonia/methane premixed flames. It was found that there was a critical point of the NH_3 mole fraction corresponding to the maximum NO_x emissions. This value was reported experimentally to be near 0.5, which was consistent with the results in the work of da Rocha et al. [38]. However, as far as NH_3/H_2/air flames are concerned, this value was measured in the range of 0.5 – 0.8 [38]. This non-monotonic trend with fuel composition was due to the synergistic results of the chemical and dilution effects arising from the introduction of hydrogen and methane. Moreover, additives like hydrogen peroxide (H_2O_2) can also dampen nitric oxide (NO) emissions [41]. Reactant humidification is another solution to suppress NO_x formation [42,43]. The addition of water reduces the flame temperature, inhibiting the NO formation rate via the reaction of $N + OH = NO + H$, thus expanding the range of the thermal DeNO$_x$ process [44,45].

The staged combustion technology has been numerically and experimentally demonstrated to reduce NO_x emissions [46–52]. An early attempt to use a secondary air injection in ammonia-fueled gas turbines occurred in the work of Somarathne et al. [31]. It was pointed out that the dilution effect primarily caused the NO reduction from the injected air, and the primary mixture should not be set too rich. In the follow-up study [46], they designed a rich-burn, quick-quench, and lean-burn combustor, inside which the fuel/oxidizer equivalence ratio in the primary and secondary injection regions can be altered. The optimum global-to-primary equivalence ratio to achieve the lowest NO emission in NH_3/air mixtures was 1.1, no matter the thermal wall condition. Based on a typical gas turbine, Kurata et al. [50] proposed a new micro-engine design scheme running on the NH_3/air mixture to optimize the emission performance. An ultra-low NO emission of 337 ppm in such a combustor was experimentally achievable, and the NH_3 and N_2O leakage can be minimized simultaneously.

While there are a few successful examples of reducing NO_x emissions in ammonia-fueled combustion, more effective but ease-of-implementation methods are still required to further eliminate this unwanted emission. Furthermore, there is little research undertaken on the role of secondary fuel injection techniques in determining NO emissions. Based on the concept of selective non-catalytic reduction technology widely applied in internal combustion engines, this work considers implementing a secondary fuel injection scheme to mitigate NO emissions in the micro-power systems. This work aims to systematically assess its applicability in the minimization of NO_x emissions and shed light on how NO formation responds to the proposed strategy. The numerical methodologies of the computational domain, model setup, and model validation are described in Section 2. In Section 3, combustion and emission performances in the absence and presence of secondary fuel injection are compared, followed by detailed analyses discussing the effects of the injection ratio and the injector axial location. Section 4 is concluded with the major findings of this work.

2. Numerical methodology

2.1. Physical model of the computational domain

A rectangular-shaped micro-combustor with a secondary fuel injection applied is numerically modeled, as depicted in Fig. 1 schematically, to evaluate the scheme of a second injection on taming NO_x emissions in ammonia combustion. The combustor is 20 mm in length, 11 mm in width, and 3 mm in height. The thicknesses of all walls are set to be 0.5 mm. The secondary fuel injector, with the length and height of 2×2 mm respectively, is implemented on the sidewall at L_1, away from the combustor inlet. Note that $\diagup$ is a dimensionless axial location of the injector signifying the ratio of the axial distance L_1 to the combustor length L. The well-premixed ammonia and oxygen with a constant temperature and pressure are injected into the primary injection region. In contrast, only ammonia is supplied from the second injection region to react with the generated NO and thus form final stable products of nitrogen. The whole combustor is assumed to be made of steel with a thermal conductivity of 16 $W{\cdot}m^{-1}{\cdot}K^{-1}$.

2.2. Model settings

Three-dimensional numerical simulations are conducted using ANSYS Fluent 2020 to provide insights into the interaction between hydrodynamics, heat transfer, pollutant formation, and chemical reactions. This interaction is calculated by solving Navier-Stokes equations of mass, momentum, energy, and species conservation. Details of the governing equations applied during numerical simulations can be found in the Fluent documentation. The SIMPLE scheme decouples the pressure–velocity coupling. The detailed chemical kinetic mechanism containing 22 species and 67 elementary reactions was originally proposed by Drake and Blint [53] and is used to describe the oxidation process of premixed ammonia/oxygen flames.

Given the relatively small Reynolds number based on the inlet velocity, the flow is assumed to be laminar, and the finite rate model is used for the chemical reactions. Our previous work details numerical assumptions such as the properties of species and mixtures, binary diffusion, and gas radiation models [54]. For completeness, only the boundary conditions are repeated here and set as follows: (1) combustor inlet – velocity inlet with a uniform velocity at atmospheric environment; (2) combustor outlet – pressure outlet; (3) outer walls – mixed thermal conditions involving the convective and radiative heat transfer [55,56]; (4) solid–fluid contact walls – no-slip shear condition and zero diffusive flux species.

In terms of the boundary conditions of the secondary injection region, ammonia with the same temperature and pressure as the primary injection one is uniformly injected into the combustor perpendicular to the $\times$ direction. That is, only a flow velocity in the y direction is applied. The amount of ammonia introduced from the secondary injector could be varying depending on the secondary injection ratio. The heat losses q from outer walls are computed as $q = h_1(T_W - T_\infty) + \varepsilon\sigma\left(T_W^4 - T_\infty^4\right)$, where h_1 denotes the convection heat transfer coefficient (20 $W{\cdot}m^{-2}{\cdot}K^{-1}$); T_W represents the outer wall temperature; T_∞ signifies the ambient temperature (300 K); ε stands for the emissivity of the outer walls (0.85);σ is the Stephan-Boltzmann constant ($5.67 \times 10^{-8} W{\cdot}m^{-2}{\cdot}K^{-4}$).

The grid independence analysis is crucial in determining a proper grid cell in simulation while ensuring relatively high computational accuracy. This is conducted by comparing the centerline OH radical and temperature on the mid-plane with three mesh resolutions in our previous studies [57]. The medium-mesh resolution, i.e., $\Delta x = 0.1mm$, and

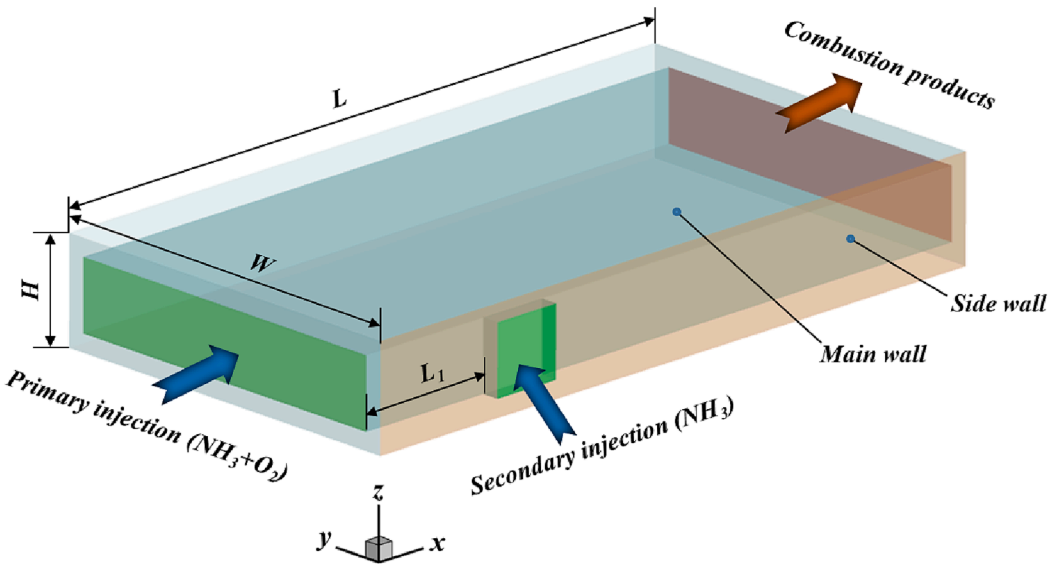

Fig. 1. The geometry of the micro-combustor with secondary fuel injection.

$\Delta y = \Delta z = 0.2mm$, is shown to sufficiently capture the flame and combustion characteristics and thus, this grid scheme is applied in the current work.

2.3. Model validation

The model predictions are first compared with experimental data from the literature to validate the computational scheme used. Only limited experimental measurements are available for ammonia-fueled micro-flames, which are considered in this work. The most relevant data were reported in the work of Zhang et al. [58]. Fig. 2 compares the experimentally obtained and numerically calculated results regarding the centerline temperature on the outer wall at two different inlet velocities (V) and equivalence ratios (ϕ). A satisfactory agreement between experimental and numerical results is observed. The largest discrepancy occurs near the combustor inlet, with a maximum value of less than

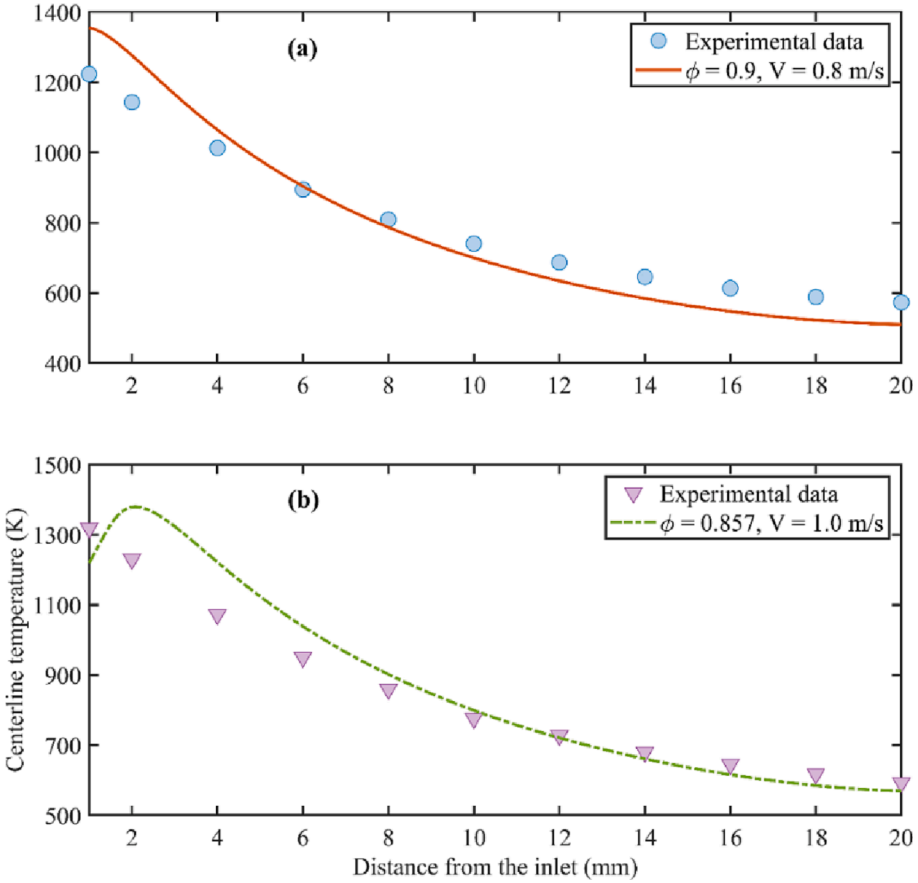

Fig. 2. Comparison of the predicted centerline temperature of the outer wall with experimental data obtained in Ref. [58].

10%. Its existence could be due to two factors. First, during the experiment, the fresh premixed mixture is continuously fed into the combustion chamber once ignited, transferring more heat to the mixing chamber connected to the combustor inlet. Second, some measurement errors exist resulting from the mass flow rate and the data acquisition system. Generally, this deviation is satisfactory, manifesting the applicability of the numerical model established in analyzing ammonia combustion.

3. Results and discussion

3.1. Comparative analysis of emission performance with/without a secondary fuel injection

In this section, we shall begin by exploring and comparing the distribution of temperature, flow field with the flame front, and NH_2 radical in the presence/absence of secondary fuel injection. Note that the fuel-oxidizer equivalence ratio at the primary injection region is set to be 1.0 for all cases considered and the flame front is denoted by 90% of the maximum OH mole fraction [59]. This is shown in Fig. 3, where $\Re$ and $\mathscr{l}$ are set to be 0.01 and 0.1, respectively, unless otherwise stated. Hereafter, the secondary fuel injection ratio ($\Re$) is defined as the ratio of the NH_3 volumetric flow rate in the secondary inlet to that of the primary inlet. It is noted that there are slight differences in the flow field, flame front, and temperature distributions except near the secondary injection region, irrespective of whether the secondary injection is applied or not. On the contrary, there is a significant difference in the predicted NH_2 concentration between the conventional combustor (CC) and the secondary injection combustor (SIC). In the SIC, a great amount of NH_2 radicals occurs downstream, mostly due to the breakdown of the injected NH_3 from the secondary inlet.

As ammonia combustion is concerned, pollutant formation such as NO and NH_3 leakage are the most critical issues as they are hazardous to the environment and human beings. Therefore, it is interesting to identify how these pollutants vary with a secondary fuel injection applied. Fig. 4 illustrates the contours of NO and NH_3 mole fractions on the cross-section in the conventional and secondary injection combustors operating under the same conditions as Fig. 3. In the conventional combustor, the NO concentration downstream of the flame front is high. In contrast, there is a region with a low NO content in the secondary injection combustor. Meanwhile, it can also be noted that NH_3 is completely consumed in the CC, as manifested by the ultra-low concentration downstream. By comparing Figs. 3 and 4, it is revealed that the change in the emission characteristics as a secondary fuel injection technique is not controlled by the temperature and flow field. Other factors need to be examined, which will be discussed in the following section.

Fig. 5 shows a comparison of NO and NH_3 emissions with a

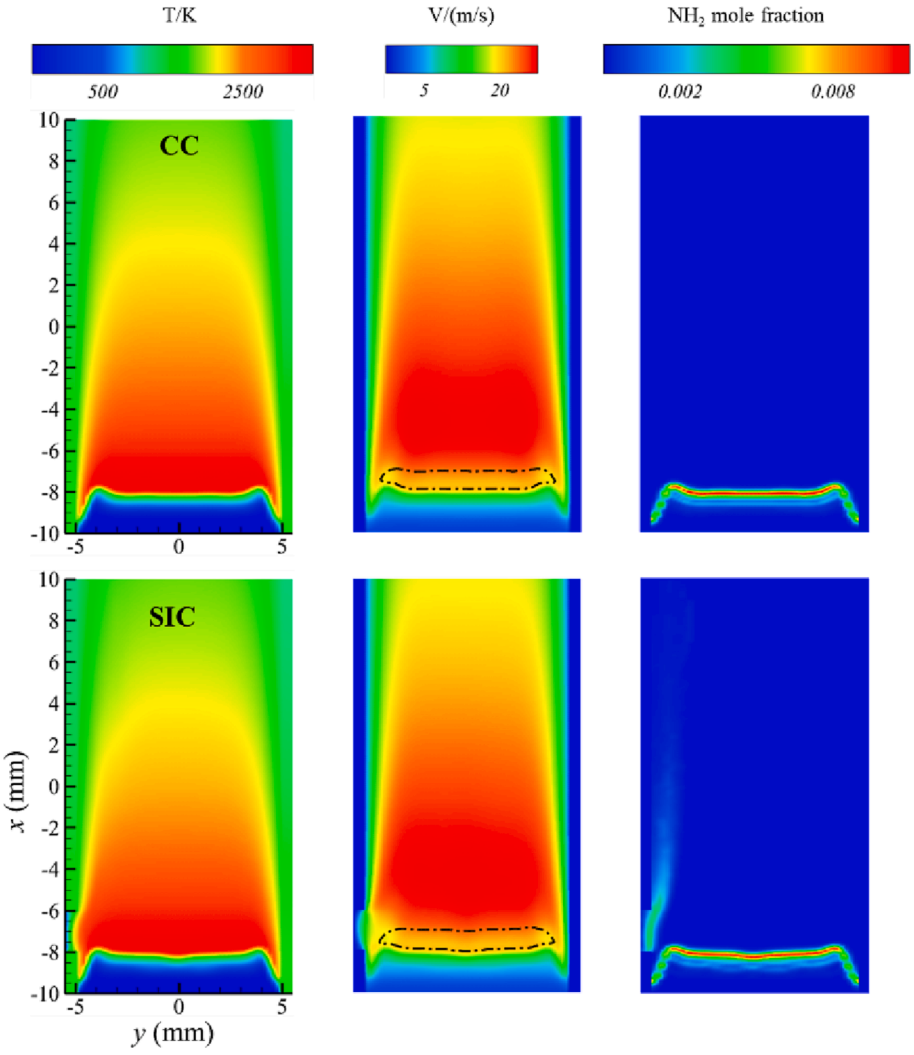

Fig. 3. Contours of temperature, velocity field overlapped with the flame front, and NH_2 mole fraction on the cross-section at the ammonia volumetric flow rate of 1200 mL/min in the conventional combustor (CC) and secondary injection combustor (SIC).

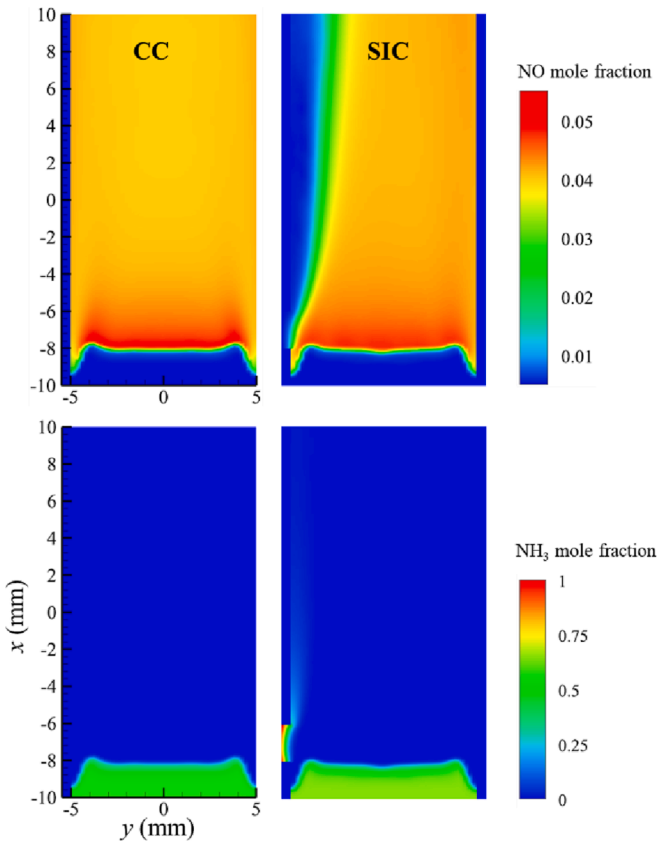

Fig. 4. Contours of NO and NH_3 mole fraction on the cross-section at the ammonia volumetric flow rate of 1200 mL/min in the conventional and secondary injection combustors.

secondary injection applied ($\Re = 0.01$ and $\not = 0.1$) or not. The NO reduction ratio is introduced to characterize the emission mitigation intensity quantitatively, and in general, it can be defined as:

$$RR_{NO} = \frac{W_{NO,CC} - W_{NO,SI}}{W_{NO,CC}} \times 100\% \quad (1)$$

where RR_{NO} signifies the NO reduction ratio, $W_{NO,CC}$ means the mole fraction of NO in the conventional combustor, and $W_{NO,SIC}$ denotes the mole fraction of NO in the secondary injection combustor.

From Fig. 5 (a), it can be seen that with the implementation of the secondary injection strategy, the mole fraction of NO at the combustor outlet exhibits a considerable decrease compared to those of the conventional combustor. As denoted by the reduction ratio, the NO emission reduction intensity is shown to be dependent on the primary fuel volumetric flow rate. The maximum reduction ratio of approximately 28% occurs at the NH_3 volumetric flow rate of 800 mL/min. Fig. 5 (b) shows that the NH_3 mole fraction in the conventional combustor is extremely low, signifying a weak NH_3 leakage. Nevertheless, as the secondary injection technique is applied, a great amount of NH_3 as high as the magnitude of 10^3 ppm is observed to run away from the combustor outlet. The NH_3 emission in the secondary injection combustor is also shown to be affected by the primary fuel flow rate. Increasing the primary fuel volumetric flow rate produces a low NH_3 leakage. When the primary NH_3 volumetric flow rate varies from 600 to 1200 mL/min, the NH_3 leakage is reduced from almost 7000 to 1000 ppm. This reduction is possibly due to the enhanced consumption rate of NH_3 reacting with NO. These results suggest that the inlet parameter is also extremely important in determining the emission performance and requires sufficient consideration.

3.2. Discussion on emission variations

To kinetically shed light on the NO mitigation mechanism with a secondary fuel injection strategy and thus enable ammonia to be run in practical combustion systems, we performed reaction pathways and rate-of-production analyses to determine the key elementary steps and the direct contributions of individual reactions that affect the formation and elimination of NO species [60]. For this, a one-dimensional premixed flame speed calculation is conducted using Chemkin-Pro 2020. Fig. 6 presents the reaction pathway diagram in a stoichiometric seeded NH_3/O_2 premixed flame operating under constant temperature and pressure conditions. For the considered conditions, NH_3 is first decomposed into NH_2 by attacking with active radicals of H (R39), O (R40), and OH (R41), where reaction R39 is the most important pathway for NH_3 consumption. These reactions are chain-branching reactions, initiating the whole combustion process.

$$NH_3 + H = NH_2 + H_2 \quad 39)$$

$$NH_3 + O = NH_2 + OH \quad 40)$$

$$NH_3 + OH = NH_2 + H_2O \quad 41)$$

The NO formation and its subsequent destruction are complex in

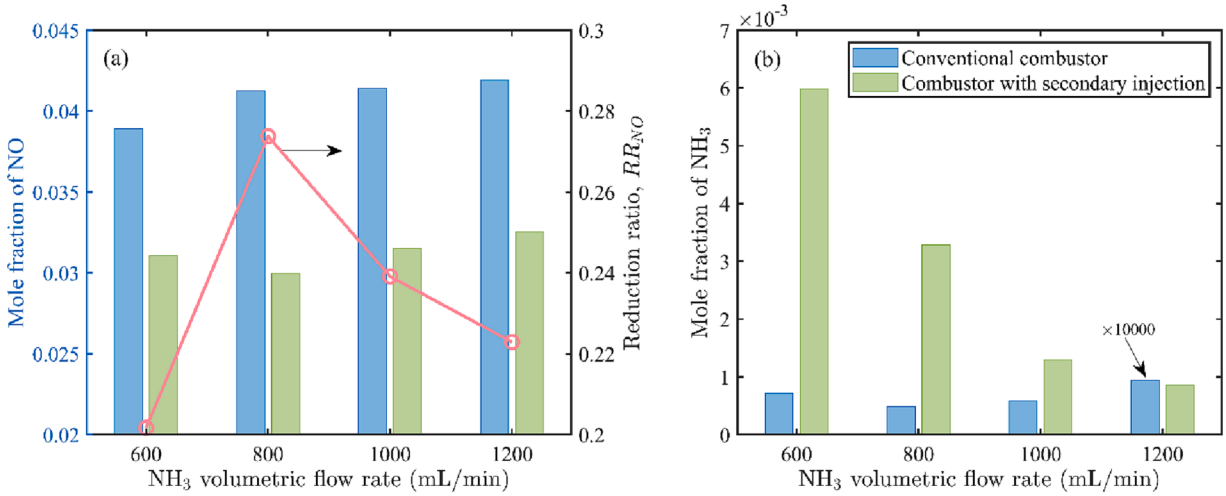

Fig. 5. A comparison of NO and NH_3 emissions at the combustor outlet in the absence/presence of secondary fuel injection, as the primary fuel flow rate is set to be four different values. Note that the mole fraction of NH_3 is multiplied by 10,000 times for clear interpretation.

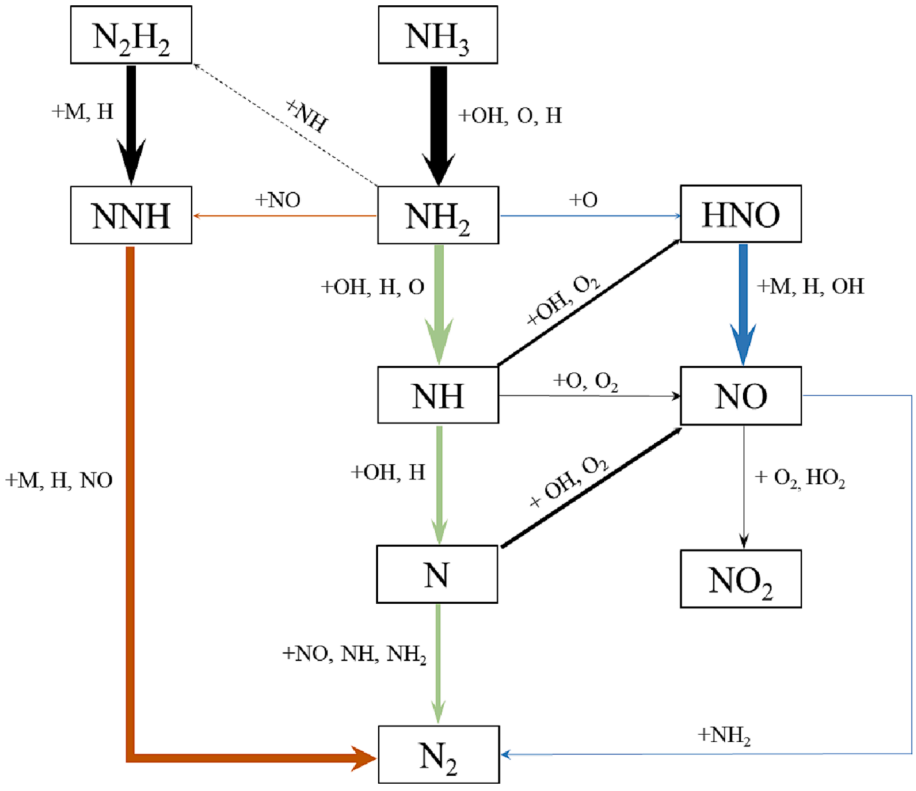

Fig. 6. Reaction pathway diagram of ammonia-oxygen premixed combustion under ambient environment.

ammonia-based combustion, mainly generated through the HNO channel [61]. The HNO formation mainly results from reactions of NH_2 with O radical, where NH reacting with OH radical and O_2 provides a secondary route. This result is per the previous demonstration [62]. The formed HNO is subsequently reacting with M (R35), H (R36), and O (R37) to generate NO, with R35 contributing the most, followed by R37.

$$HNO + M = H + NO + M \quad 35)$$

$$HNO + H = H_2 + NO \quad 36)$$

$$HNO + OH = NO + H_2O \quad 37)$$

Fig. 7 illustrates the most important top 15 elementary reaction steps that control the formation and destruction of NO species in the atmospheric operating environment based on the rate-of-production analysis. The abscissa denotes the gas flow direction. Under the conditions examined, the significant contributions to the NO formation are made by reactions of HNO with M and OH. This is consistent with previous work, even when using a different reaction mechanism [35]. As far as NO destruction is concerned, it is mainly consumed through the following five reaction channels. In ammonia combustion, the reaction rate of these steps is expected to be varied with secondary fuel injection applied, thus chemically affecting the emission characteristics.

$$O + N_2 = N + NO \quad 28)$$

$$NH_2 + NO = N_2 + H_2O \quad 47)$$

$$NNH + NO = N_2 + HNO \quad 60)$$

$$NH_2 + NO = NNH + OH \quad 62)$$

$$NH + NO = N_2O + H \quad 63)$$

Having determined the important NO destruction channel, examining how the reaction rates vary with the introduction of secondary fuel

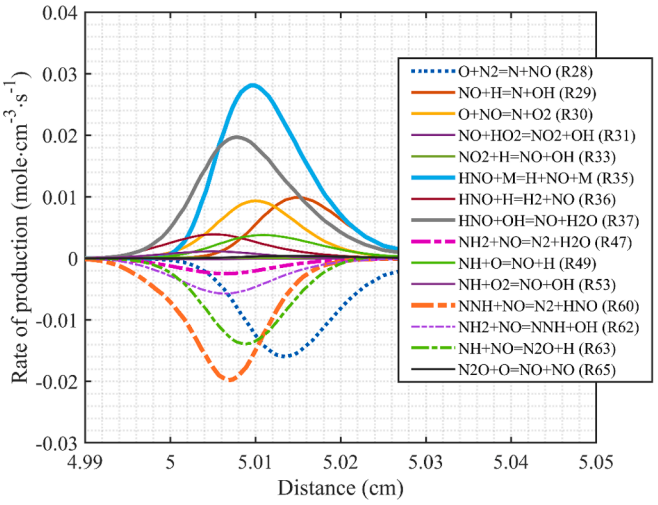

Fig. 7. Rates of production of the most important top 15 elementary reaction steps controlling the formation and destruction of NO species.

injection is of prime importance. Fig. 8 shows the contours of the kinetic rate of these five reactions in the secondary injection combustor. In light of the negligible discrepancy in the calculated radical distributions near the flame region, the reaction rate herein in the conventional combustor is not included. Note that the negative value of the R28 reaction rate denotes that this is a backward-dominant reaction step. Of these NO consumption steps, reactions R28 and R63 have the largest reaction rate, suggesting that these steps contribute most to the NO removal as the secondary fuel injection is applied. Comparing Figs. 3 and 8, it can be concluded that the physical effects such as temperature and flow field change caused by the implementation of secondary fuel injection are not the major contributors to the NO emission suppression. In contrast, the

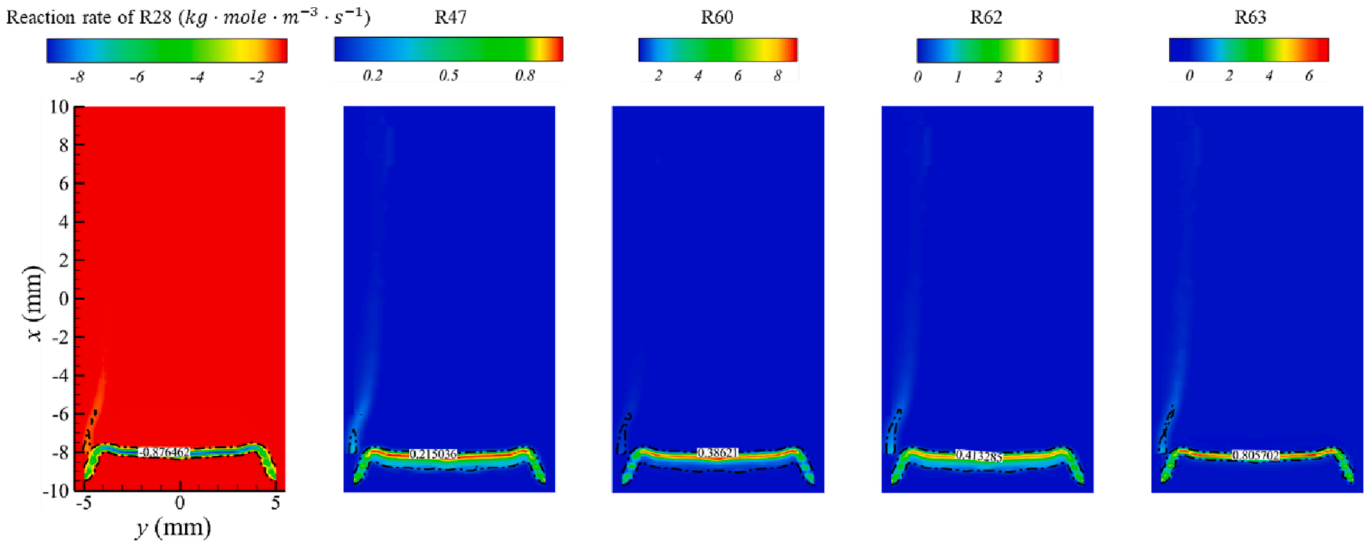

Fig. 8. Contours of the reaction rate of the most important NO destruction on the cross-section.

chemical effect is the predominant factor.

3.3. Parametric studies

As stated previously, the NO and NH_3 emissions depend on the primary fuel flow rate. Despite the relatively significant reduction in the NO emission with a secondary injection technique, a huge amount of NH_3 could leak, which is undesirable. Therefore, it is expected that the secondary injection design parameter plays a key role in the combustion characteristics and merits investigation. Further studies are conducted on the combustor with a secondary fuel injection by gradually changing the injection ratio and the axial injection location.

3.3.1. Effect of the secondary fuel injection ratio

To have a better understanding of how the concentration of the secondary fuel injection affects the emission behavior, six sets of fuel injection ratios, i.e., $\Re$ = 0.001, 0.002, 0.01, 0.02, 0.05, and 0.1, are considered at the primary NH_3 volumetric flow rate of 1200 mL/min and χ = 0.1. First, we examine the distributions of NO and NH_3 mole fractions on the cross-section in these two combustor configurations. The corresponding results are illustrated in Fig. 9. An observation of NO distributions shows that a low NO concentration region is highly dependent on the secondary fuel injection ratio. With an increase in the $\Re$, signifying the increasing concentration of NH_3 in the combustion zone, this region is further widened, which can manifest a low NO emission. However, the NH_3 distribution presents an opposite trend with

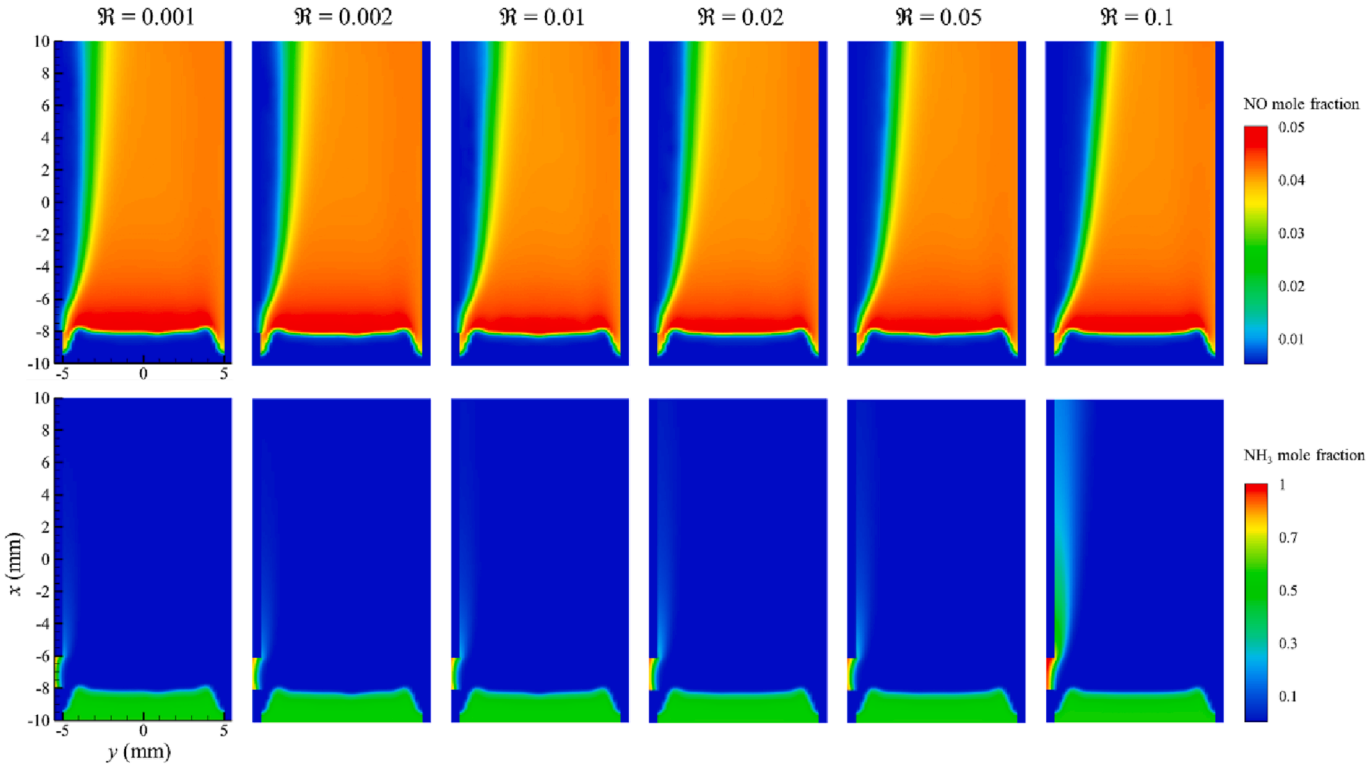

Fig. 9. The distributions of NO and NH_3 mole fractions with varied secondary fuel injection ratios.

the fuel injection ratio. This phenomenon is not favorable for practical combustion devices.

The predicted NO, and NH_3 mole fractions on the combustor outlet operating under the same circumstance in Fig. 9 have been computationally calculated, as shown in Fig. 10. It is seen that the NO formation has a monotonic dependence on the $\Re$, and increasing it gives rise to a low NO emission. Nevertheless, this is accompanied by a negative effect in higher NH_3 leakage. The NH_3 leakage can be either negligible or notable, depending on the injection ratio. When $\Re = 0.001$ or 0.002, the NH_3 emission is as low as several ppm. In practice, this is desirable as it complies with the stringent emission regulation.

Further increasing $\Re$ to 0.02 results in the NH_3 leakage being almost 900 ppm, becoming much more notable as $\Re$ approaches 0.05. This increase is mostly due to weakening NH_3 conversion performance because of the high concentrations. A comparison and discussion on NO and NH_3 leakage imply the existence of a critical fuel injection ratio where the NO can be significantly attenuated with NH_3 leakage maintaining within the acceptable range.

As discussed above, NH_2 is the first product from the breakdown of the injected NH_3 from the secondary injector and an important intermediate species initiating the NO consumption process. Thus, it is meaningful to examine how the NH_2 concentration varies with the secondary fuel injection ratio $\Re$. Fig. 11 shows the contours of the NH_2 mole fraction on the cross-section under different $\Re$. It is seen that $\Re$ has an important effect on the NH_2 distribution. The region of a high NH_2 radical downstream of the secondary injection is observed to be extended with increased $\Re$. This phenomenon is expectable, and the increasing NH_2 contributes to consuming the NO radical through the destruction reaction steps, as previously mentioned in Figs. 7 and 8. This further explains the variation of NO formation in Fig. 10.

3.3.2. *Effect of the dimensionless axial location of the secondary fuel injection*

The previous results reveal that once $\Re$ approaches 0.002, the NH_3 leakage is extremely low, and further decreasing $\Re$ does not improve NH_3 reduction performance. Now, let us examine the effect of the axial location of the secondary fuel injection on the emission behavior with $\Re = 0.002$. The variation of NO and NH_3 mole fractions on the combustor outlet has been computationally determined over extensive ranges of χ from 0.1 to 0.5 at the primary NH_3 volumetric flow rate of 1200 mL/min, as shown in Fig. 12. The predicted NO emission is shown to reduce marginally as the secondary injection gradually moves from upstream to downstream of the combustor, manifesting a weak dependence of NO formation/destruction on the injection location. As far as the NH_3 leakage is concerned, it exhibits an almost linear relationship with χ. In other words, increasing χ is more likely to give rise to a high NH_3 leakage at the combustor outlet. This reveals the key role in the NH_3 emission being played by the axial secondary injection location.

Considering the minimal change in the NO emission with the axial location of the secondary fuel injection, we shall only examine the NH_3 distribution to show how the secondary injection location affects its formation. The corresponding results are shown in Fig. 13, where the operating condition is the same as that in Fig. 12. For all investigated cases, there is a region of NH_3 downstream of the secondary fuel injection. Still, the region's size tends to vary with the axial injection location and the NH_3 concentration. Specifically, with $\chi = 0.1$, the region of a high NH_3 concentration is the smallest, and little NH_3 leakage is observed near the combustor outlet. This suggests that NH_3 is almost completely consumed and converted into final products like N_2. However, as χ is increased, demonstrating that the secondary injection is approaching downstream, that region is gradually becoming larger, and finally, there is some runaway of NH_3 from the combustor outlet. These results reveal that the axial location of secondary fuel injection is extremely important in determining NH_3 emissions, and it should not be placed too far away from the combustor inlet.

4. Conclusions

This work proposes a secondary fuel injection strategy to attenuate NO_x emissions in ammonia-fueled combustion systems, and its applicability to emission mitigation is evaluated and discussed in detail. Extensive three-dimensional simulations involving detailed kinetic chemistry are conducted on premixed ammonia/oxygen micro-combustors. The combustion and emission performances with secondary fuel injection applied are first identified and compared to conventional combustion. Then, the roles of key parameters relating to the

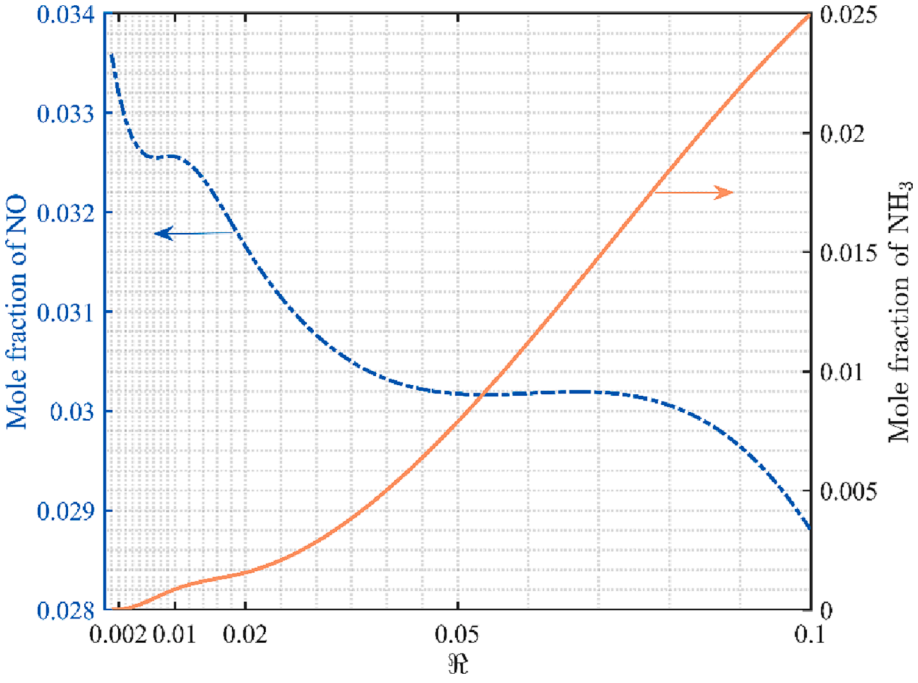

Fig. 10. The variation of NO and NH_3 mole fractions at the combustor outlet as a function of the secondary fuel injection ratio.

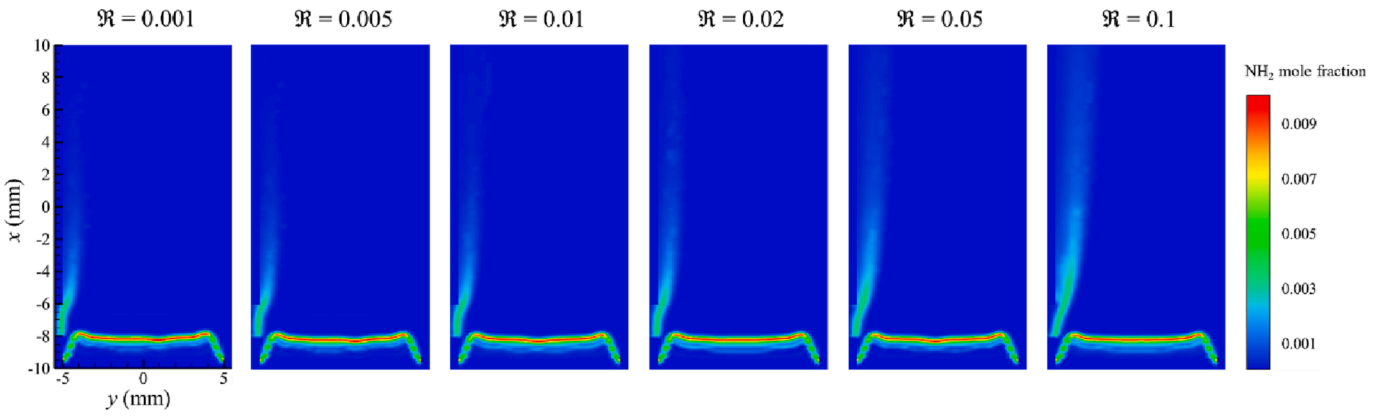

Fig. 11. Distributions of NH_2 mole fraction on the cross-section varied with $\Re$.

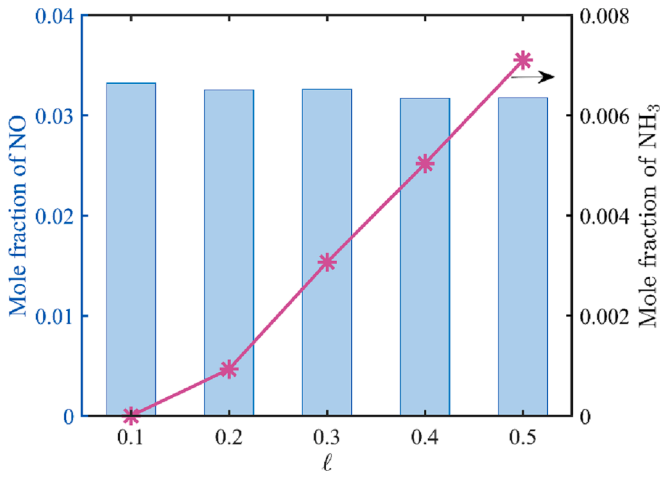

Fig. 12. The variation of NO and NH_3 mole fractions emitted at the combustor outlet as a function of the axial location of the secondary fuel injection.

secondary injection strategy in affecting NO_x formation and NH_3 leakage are analyzed. The underlying mechanism leading to the emission reduction is kinetically confirmed. The main findings are summarized as follows:

(1) The introduction of secondary fuel injection is extremely effective in damping NO_x generation. A nearly 28% reduction in NO emission is achieved with an NH_3 leakage of less than 900 ppm, as the secondary fuel injection ratio $\Re$ and dimensionless axial location ℓ are set to be 0.01 and 0.1, respectively.

(2) The key reaction steps affecting NO formation/destruction are confirmed by utilizing the reaction pathway and rate-of-production analysis. Coupling these elementary reactions with three-dimensional calculations enables the steps contributing most to the NO removal to be identified, thus highlighting the significance of the chemical effect in the pollutant suppression arising from the implementation of NH_3 secondary injection.

(3) The emission control effectiveness is found to vary with the selection of the secondary fuel injection ratio $\Re$. Elevating $\Re$ facilitates a low NO emission but results in an increased NH_3 leakage. The NH_3 runaway can be either negligible or notable depending on the fuel injection ratio. A threshold of the injection ratio exists where the NO emission is extremely low and the NH_3 leakage is within a desirable range.

(4) For a specified secondary fuel injection ratio, the dimensionless axial location of the secondary injector ℓ plays a minimal role in the NO formation. Still, it can affect the NH_3 emission to some extent. Increasing ℓ is more likely to result in a high NH_3 leakage. The secondary fuel injection should not be placed too far away from the combustor inlet for a low pollutant emission.

In summary, this work demonstrates the successful application of a secondary fuel injection strategy to tame NO emissions with ultra-low NH_3 leakage in ammonia micro-combustion systems. This strategy also applies to large-scale combustion devices, such as the furnace, boilers,

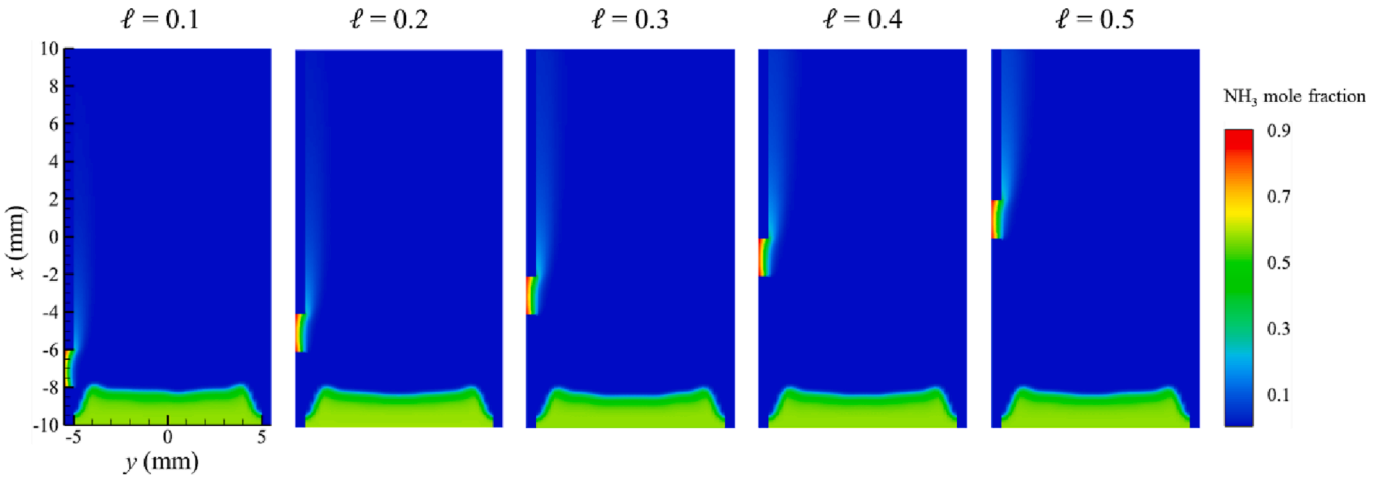

Fig. 13. Distributions of NH_3 mole fraction on the cross-section varied with the axial location of the secondary fuel injection.

and land-based gas turbines, when fully or partially fueled with ammonia in the transition to a low-carbon economy.

Credit author statement

Tao Cai: Investigation, Software, Methodology, Validation, Formal analysis, Writing – original draft. **Dan Zhao:** Conceptualization, Supervision, Funding acquisition, Project administration, Writing – review and editing. **Lin Ji:** Methodology, Writing – review & editing. **Avinash Kumar Agarwal:** Formal analysis, Writing – review & editing.

Declaration of Competing Interest

The authors declare that they have no known competing financial interests or personal relationships that could have appeared to influence the work reported in this paper.

Data availability

Data will be made available on request.

Acknowledgments

We gratefully acknowledge the financial support provided by the University of Canterbury, New Zealand (grant no. CPS20-03-002, grant no. 452DISDZ) and National Research Foundation Singapore (grant no. NRF2016 NRF-NSFC001-102). TC would like to thank the College of Engineering, the University of Canterbury, for providing his PhD studentship.

References

[1] Cai T, Zhao D, Gutmark E. Overview of fundamental kinetic mechanisms and emission mitigation in ammonia combustion. Chem Eng J 2023;458:141391.
[2] Tan D, Wu Y, Lv J, Li J, Ou X, Meng Y, et al. Performance optimization of a diesel engine fueled with hydrogen/biodiesel with water addition based on the response surface methodology. Energy 2023;263:125869.
[3] Tan D, Meng Y, Tian J, Zhang C, Zhang Z, Yang G, et al. Utilization of renewable and sustainable diesel/methanol/n-butanol (DMB) blends for reducing the engine emissions in a diesel engine with different pre-injection strategies. Energy 2023;269:126785.
[4] Valera-Medina A, Xiao H, Owen-Jones M, David WI, Bowen P. Ammonia for power. Prog Energy Combust Sci 2018;69:63–102.
[5] Zhang Z, Li J, Tian J, Dong R, Zou Z, Gao S, et al. Performance, combustion and emission characteristics investigations on a diesel engine fueled with diesel/ethanol/n-butanol blends. Energy 2022;249:123733.
[6] Yapicioglu A, Dincer I. A review on clean ammonia as a potential fuel for power generators. Renew Sustain Energy Rev 2019;103:96–108.
[7] MacFarlane DR, Cherepanov PV, Choi J, Suryanto BHR, Hodgetts RY, Bakker JM, et al. A roadmap to the ammonia economy. Joule 2020;4(6):1186–205.
[8] Cai T, Zhao D, Li X, Shi B, Li J. Mitigating NOx emissions from an ammonia-fueled micro-power system with a perforated plate implemented. J Hazard Mater 2021;401:123848.
[9] Burrows L, Gao P-X, Bollas GM. Thermodynamic feasibility analysis of distributed chemical looping ammonia synthesis. Chemical Engineering Journal 2021;426:131421.
[10] Service R. Ammonia—a renewable fuel made from sun, air, and water—could power the globe without carbon. Science 2018:aau7489.
[11] Sánchez A, Martín M. Optimal renewable production of ammonia from water and air. J Clean Prod 2018;178:325–42.
[12] Morawski AW, Ćmielewska K, Ekiert E, Kusiak-Nejman E, Pełech I, Staciwa P, et al. Effective green ammonia synthesis from gaseous nitrogen and CO2 saturated-water vapour utilizing a novel photocatalytic reactor. Chem Eng J 2022;446:137030.
[13] Han X, Wang Z, He Y, Liu Y, Zhu Y, Konnov AA. The temperature dependence of the laminar burning velocity and superadiabatic flame temperature phenomenon for NH3/air flames. Combust Flame 2020;217:314–20.
[14] Hayakawa A, Goto T, Mimoto R, Arakawa Y, Kudo T, Kobayashi H. Laminar burning velocity and Markstein length of ammonia/air premixed flames at various pressures. Fuel 2015;159:98–106.
[15] Liu Q, Chen X, Huang J, Shen Y, Zhang Y, Liu Z. The characteristics of flame propagation in ammonia/oxygen mixtures. J Hazard Mater 2019;363:187–96.
[16] Sun Y, Zhao D, Ji C, Zhu T, Rao Z, Wang B. Large-eddy simulations of self-excited thermoacoustic instability in a premixed swirling combustor with an outlet nozzle. Physics of Fluids 2022;34(4):044112.
[17] Zhao D, Guan Y. Characterizing modal exponential growth behaviors of self-excited transverse and longitudinal thermoacoustic instabilities. Physics of Fluids 2022;34(2):024109.
[18] Li J, Huang H, Kobayashi N, He Z, Osaka Y, Zeng T. Numerical study on effect of oxygen content in combustion air on ammonia combustion. Energy 2015;93:2053–68.
[19] Zhang M, Wei X, Wang J, Huang Z, Tan H. The blow-off and transient characteristics of co-firing ammonia/methane fuels in a swirl combustor. Proc Combust Inst 2021;38(4):5859–68.
[20] Cai T, Zhao D. Enhancing and assessing ammonia-air combustion performance by blending with dimethyl ether. Renewable and Sustainable Energy Reviews 2022;156:112003.
[21] Cai T, Zhao D, Chan SH, Shahsavari M. Tailoring reduced mechanisms for predicting flame propagation and ignition characteristics in ammonia and ammonia/hydrogen mixtures. Energy 2022;260:125090.
[22] Wu F-H, Chen G-B. Numerical study of hydrogen peroxide enhancement of ammonia premixed flames. Energy 2020;209:118118.
[23] Sun X, Xie M, Zhou F, Wu X, Fu J, Liu J. Hierarchical evolutionary construction of neural network models for an Atkinson cycle engine with double injection strategy based on the PSO-Nadam algorithm. Fuel 2023;333:126531.
[24] Zhang Z, Dong R, Lan G, Yuan T, Tan D. Diesel particulate filter regeneration mechanism of modern automobile engines and methods of reducing PM emissions: A review. Environ Sci Pollut Res 2023.
[25] Zhang Z, Ye J, Tan D, Feng Z, Luo J, Tan Y, et al. The effects of Fe2O3 based DOC and SCR catalyst on the combustion and emission characteristics of a diesel engine fueled with biodiesel. Fuel 2021;290:120039.
[26] Okafor EC, Yamashita H, Hayakawa A, Somarathne KKA, Kudo T, Tsujimura T, et al. Flame stability and emissions characteristics of liquid ammonia spray co-fired with methane in a single stage swirl combustor. Fuel 2021;287:119433.
[27] Ni S, Zhao D, You Y, Huang Y, Wang B, Su Y. NOx emission and energy conversion efficiency studies on ammonia-powered micro-combustor with ring-shaped ribs in fuel-rich combustion. Journal of Cleaner Production 2021;320:128901.
[28] Medhat M, Yehia M, Khalil A, Franco MC, Rocha RC. A numerical prediction of stabilized turbulent partially premixed flames using ammonia/hydrogen mixture. J Adv Res Fluid Mech Thermal Sci 2021;87(3):113–33.
[29] Brackmann C, Alekseev VA, Zhou B, Nordström E, Bengtsson P-E, Li Z, et al. Structure of premixed ammonia+ air flames at atmospheric pressure: Laser diagnostics and kinetic modeling. Combust Flame 2016;163:370–81.
[30] Honzawa T, Kai R, Okada A, Valera-Medina A, Bowen PJ, Kurose R. Predictions of NO and CO emissions in ammonia/methane/air combustion by LES using a non-adiabatic flamelet generated manifold. Energy 2019;186:115771.
[31] Somarathne KDKA, Hatakeyama S, Hayakawa A, Kobayashi H. Numerical study of a low emission gas turbine like combustor for turbulent ammonia/air premixed swirl flames with a secondary air injection at high pressure. Int J Hydrogen Energy 2017;42(44):27388–99.
[32] Hayakawa A, Goto T, Mimoto R, Kudo T, Kobayashi H. NO formation/reduction mechanisms of ammonia/air premixed flames at various equivalence ratios and pressures. Mech Eng J 2015:14–00402.
[33] Tang Y, Xie D, Shi B, Wang N, Li S. Flammability enhancement of swirling ammonia/air combustion using AC powered gliding arc discharges. Fuel 2022;313:122674.
[34] Choe J, Sun W, Ombrello T, Carter C. Plasma assisted ammonia combustion: Simultaneous NOx reduction and flame enhancement. Combust Flame 2021;228:430–2.
[35] Zhang X, Moosakutty SP, Rajan RP, Younes M, Sarathy SM. Combustion chemistry of ammonia/hydrogen mixtures: Jet-stirred reactor measurements and comprehensive kinetic modeling. Combustion and Flame 2021;234:111653.
[36] Ramos CF, Rocha RC, Oliveira PM, Costa M, Bai X-S. Experimental and kinetic modelling investigation on NO, CO and NH3 emissions from NH3/CH4/air premixed flames. Fuel 2019;254:115693.
[37] da Rocha RC, Costa M, Bai X-S. Chemical kinetic modelling of ammonia/hydrogen/air ignition, premixed flame propagation and NO emission. Fuel 2019;246:24–33.
[38] Rocha RC, Ramos CF, Costa M, Bai X-S. Combustion of NH3/CH4/Air and NH3/H2/air mixtures in a porous burner: Experiments and kinetic modeling. Energy Fuel 2019;33(12):12767–80.
[39] Li Z, Li S. Kinetics modeling of NOx emissions characteristics of a NH3/H2 fueled gas turbine combustor. Int J Hydrogen Energy 2021;46(5):4526–37.
[40] Han L, Li J, Zhao D, Xi Y, Gu X, Wang N. Effect analysis on energy conversion enhancement and NOx emission reduction of ammonia/hydrogen fuelled wavy micro-combustor for micro-thermophotovoltaic application. Fuel 2021;289:119755.
[41] Khalil AT, Manias DM, Kyritsis DC, Goussis DA. NO formation and autoignition dynamics during combustion of H2O-diluted NH3/H2O2 mixtures with air. Energies 2021;14(1):84.
[42] Božo MG, Vigueras-Zuniga M, Buffi M, Seljak T, Valera-Medina A. Fuel rich ammonia-hydrogen injection for humidified gas turbines. Applied Energy 2019;251:113334.
[43] Sun Z, Xu J, Su S, Qing M, Wang L, Cui X, et al. Formation and reduction of NO from the oxidation of NH3/CH4 with high concentration of H2O. Fuel 2019;247:19–25.
[44] Javed MT, Irfan N, Gibbs B. Control of combustion-generated nitrogen oxides by selective non-catalytic reduction. J Environ Manage 2007;83(3):251–89.
[45] Pugh D, Bowen P, Valera-Medina A, Giles A, Runyon J, Marsh R. Influence of steam addition and elevated ambient conditions on NOx reduction in a staged premixed swirling NH3/H2 flame. Proc Combust Inst 2019;37(4):5401–9.

[46] Somarathne KDKA, Okafor EC, Hayakawa A, Kudo T, Kurata O, Iki N, et al. Emission characteristics of turbulent non-premixed ammonia/air and methane/air swirl flames through a rich-lean combustor under various wall thermal boundary conditions at high pressure. Combust Flame 2019;210:247–61.
[47] Okafor EC, Tsukamoto M, Hayakawa A, Somarathne KDKA, Kudo T, Tsujimura T, et al. Influence of wall heat loss on the emission characteristics of premixed ammonia-air swirling flames interacting with the combustor wall. Proc Combust Inst 2021;38(4):5139–46.
[48] Pacheco GP, Rocha RC, Franco MC, Mendes MAA, Fernandes EC, Coelho PJ, et al. Experimental and kinetic investigation of stoichiometric to rich NH3/H2/Air flames in a swirl and bluff-body stabilized burner. Energy Fuel 2021;35(9):7201–16.
[49] Rocha RC, Costa M, Bai X-S. Combustion and emission characteristics of ammonia under conditions relevant to modern gas turbines. Combust Sci Technol 2021;193(14):2514–33.
[50] Kurata O, Iki N, Inoue T, Matsunuma T, Tsujimura T, Furutani H, et al. Development of a wide range-operable, rich-lean low-NOx combustor for NH3 fuel gas-turbine power generation. Proc Combust Inst 2019;37(4):4587–95.
[51] Li Z, Li S. Effects of inter-stage mixing on the NOx emission of staged ammonia combustion. Int J Hydrogen Energy 2022;47(16):9791–9.
[52] Somarathne KDKA, Okafor EC, Sugawara D, Hayakawa A, Kobayashi H. Effects of OH concentration and temperature on NO emission characteristics of turbulent non-premixed CH4/NH3/air flames in a two-stage gas turbine like combustor at high pressure. Proc Combust Inst 2021;38(4):5163–70.
[53] Drake MC, Blint RJ. Thermal NOx in stretched laminar opposed-flow diffusion flames with CO/H2/N2 fuel. Combust Flame 1989;76(2):151–67.
[54] Cai T, Zhao D, Wang B, Li J, Guan Y. NOx emission and thermal performances studies on premixed ammonia-oxygen combustion in a CO2-free micro-planar combustor. Fuel 2020;280:118554.
[55] Peng Q, Yang W, Jiaqiang E, Li Z, Xu H, Fu G, et al. Investigation on H2/air combustion with C3H8 addition in the combustor with part/full porous medium. Energy Convers Manage 2021;228:113652.
[56] Tang A, Deng J, Cai T, Xu Y, Pan J. Combustion characteristics of premixed propane/hydrogen/air in the micro-planar combustor with different channel-heights. Appl Energy 2017;203:635–42.
[57] Cai T, Becker SM, Cao F, Wang B, Tang A, Fu J, et al. NOx emission performance assessment on a perforated plate-implemented premixed ammonia-oxygen micro-combustion system. Chem Eng J 2021;417:128033.
[58] Zhang Y, Lu Q, Fan B, Quaye EK, Weng J, Xiao S, et al. Effect of intake method on ammonia/oxygen non-premixed combustion in the micro combustor with dual-inlet. Fuel 2022;317:123504.
[59] Cai T, Tang A, Zhao D, Zhou C, Huang Q. Flame dynamics and stability of premixed methane/air in micro-planar quartz combustors. Energy 2020;193:116767.
[60] Xiao H, Valera-Medina A, Bowen PJ. Study on premixed combustion characteristics of co-firing ammonia/methane fuels. Energy 2017;140:125–35.
[61] Kobayashi H, Hayakawa A, Somarathne KKA, Okafor EC. Science and technology of ammonia combustion. Proc Combust Inst 2019;37(1):109–33.
[62] Lindstedt R, Lockwood F, Selim M. Detailed kinetic modelling of chemistry and temperature effects on ammonia oxidation. Combust Sci Technol 1994;99(4–6):253–76.